Journal of Solid State Chemistry 184 (2011) 64–69

Contents lists available at ScienceDirect

Journal of Solid State Chemistry

journal homepage: www.elsevier.com/locate/jssc

Ca-for-Sr substitution in the thermoelectric $[(Sr,Ca)_2(O,OH)_2]_q[CoO_2]$ misfit-layered cobalt-oxide system

Hisao Yamauchi [a,b], Lassi Karvonen [a], Takayuki Egashira [b], Yoshiaki Tanaka [b], Maarit Karppinen [a,b,*]

[a] Laboratory of Inorganic Chemistry, Department of Chemistry, Aalto University, FI-00076 AALTO, Finland
[b] Materials and Structures Laboratory, Tokyo Institute of Technology, Yokohama 226-8503, Japan

ARTICLE INFO

Article history:
Received 4 June 2010
Received in revised form
1 October 2010
Accepted 16 October 2010
Available online 23 October 2010

Keywords:
Thermoelectrics
Misfit-layered structure
Cobalt oxides
Isovalent substitution

ABSTRACT

Calcium-for-strontium substituted samples of the misfit-layered cobalt-oxide system, $[(Sr_{1-x}Ca_x)_2(O,OH)_2]_q[CoO_2]$, were successfully synthesized up to $x=0.2$ with a sample-encapsulation technique originally developed for the $x=0$ end phase. While the $x=0$ sample has a commensurate match between the two layer blocks (i.e. $q=0.5$), isovalent Ca-for-Sr substitution induces lattice misfit (i.e. $q>0.5$). At the same time the Seebeck coefficient gets increased, but the increase in resistivity results in suppressing the thermoelectric power factor. The magnetic anomaly in the $x=0$ sample gets released upon the Ca substitution for the $x=0.2$ sample to exhibit an almost Curie–Weiss behavior. It is concluded that with increasing x in $[(Sr_{1-x}Ca_x)_2(O,OH)_2]_q[CoO_2]$ the properties smoothly evolve towards those previously reported for the $x=1.0$ end member, $[Ca_{1.7}O_{2.1}H_{2.4}]_{0.58}[CoO_2]$.

1. Introduction

Since synthesized for the first time in late 1990s [1,2] misfit-layered (ML) cobalt oxides have been in the very focus of research interest from both scientific and technological points of view. The interest arises from the fact that they – like the related Na_xCoO_2 system [3] – have been found to exhibit exceptionally high values of the thermoelectric figure-of-merit, $Z\ (\equiv S^2/\kappa\rho)$ [4–7]. Here it should be emphasized that the high Z value requires the material to be simultaneously a good electrical conductor (with low resistivity, ρ) and a poor thermal conductor (with low thermal conductivity, κ), and, moreover, to possess a large thermoelectric power or Seebeck coefficient (S). This combination is not possible for conventional materials and it is the unique crystal structure of the ML compounds that makes it possible for them to simultaneously possess the properties somewhat contradictory from conventional view points.

Misfit-layered cobalt oxides – described with the general formula, $[M_mA_2O_{m+2}]_q[CoO_2]$ (M=Co, Bi, Pb, Tl, etc.; A=Ca, Sr, Ba, etc.; $m=0$, 1, 2; $q\geq 0.5$) – possess a layered crystal structure consisting of two types of layer block: hexagonal $[CoO_2]$ block and rock-salt-structured $[M_mA_2O_{m+2}]$ block which are stacked incoherently to each other forming a kind of composite crystal. While the number of M-cation layers in $[M_mA_2O_{m+2}]$ is defined by m, the "misfit parameter" $q\ (\equiv b_H/b_{RS}$ with b_H and b_{RS} being the b lattice parameters of the two types of layer blocks along which the layers are by definition misfitting and to which the layer-stacking direction is perpendicular) is a measure of the mismatch between the two blocks, a commensurate structure appearing only at $q=0.5$ (or 1.0). The hexagonal $[CoO_2]$ layer, consisting of CoO_6 polyhedra sharing edges, is the basic building block existing in all ML cobalt oxides (see Fig. 1). Recently high-quality samples of pure CoO_2 phase were successfully prepared (through electrochemical delithiation of Li_xCoO_2) and characterized [8–10], but this phase constituting of consecutively stacked $[CoO_2]$ layers is highly unstable. Stabilization of such hexagonal $[CoO_2]$ layers containing high-valent (i.e. Co^{IV}) cobalt requires that the layers are separated either with a single plane of alkaline metal ions between them, as in Na_xCoO_2 [11] and Li_xCoO_2 [12], or with a rock-salt structured $[AO–(MO)_m–AO]$ block, as in the very ML cobalt oxides. In these cases the separation layer is either nonstoichiometric or incommensurate with respect to the $[CoO_2]$ layer, i.e. $0<x<1$ in $(Li/Na)_xCoO_2$ and $0.5<q<1.0$ in $[M_mA_2O_{m+2}]_q[CoO_2]$.

The attractive Seebeck property of the ML cobalt oxides originates from the spin and orbital entropy of tetravalent low-spin cobalt (Co^{IV}) in the $[CoO_2]$ layer induced by the charge of the $[M_mA_2O_{m+2}]$ block [13]. It should also be noted that Co^{IV} among Co^{III} yields a hole which makes the $[CoO_2]$ layer a metallic conductor. Moreover, the poor or misfit inter-block connection between the conducting $[CoO_2]$ layer and the insulating rock-salt $[M_mA_2O_{m+2}]$ block effectively suppresses the thermal and electrical transport perpendicular to the layers [14]. Besides acting as a kind of transport barrier and moderator for the charge carriers, the rock-salt $[M_mA_2O_{m+2}]$ block also offers means to regulate the charge carrier concentration in the $[CoO_2]$ layers, yet leaving them largely

* Corresponding author at: Laboratory of Inorganic Chemistry, Department of Chemistry, Aalto University, P.O. Box 16100, FI-00076 AALTO, Finland.
Fax: +358 9 462 373.
E-mail address: maarit.karppinen@tkk.fi (M. Karppinen).

0022-4596/$ - see front matter © 2010 Elsevier Inc. All rights reserved.
doi:10.1016/j.jssc.2010.10.028

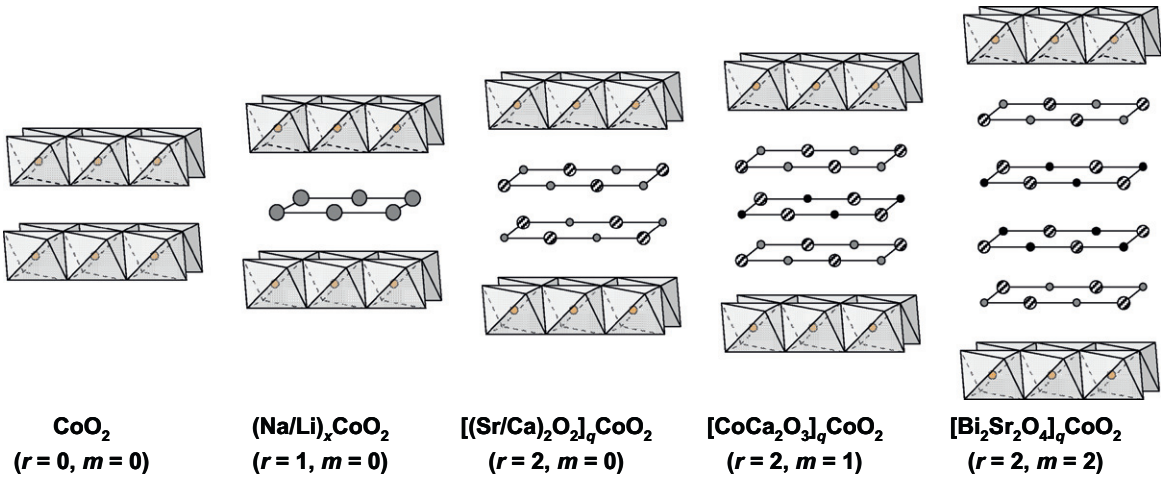

Fig. 1. Schematic illustration of the crystal structures of misfit-layered cobalt oxides and related $[M_mA_rO_{m+r}]_q[CoO_2]$ phases based on the hexagonal $[CoO_2]$ layer. Illustration of the atoms in the rock-salt layer: (Gray) *A*: Na, Li, Ca or Sr; (Black) *M*. Co or Bi; (Shaded) O.

intact, as it exclusively allows, e.g. oxygen-content tuning [15,16] and various cation substitutions [17].

All the known members of the ML $[M_mA_2O_{m+2}]_q[CoO_2]$ family possessed a stoichiometry/crystal structure corresponding to $m=1$ or 2 (Fig. 1), until recently the "zero" or $m=0$ ML phases, i.e. $[Sr_2O_2]_q[CoO_2]$ [18,19] and $[Ca_2O_2]_q[CoO_2]$ [20,21], were synthesized. While the ideal formulae of these zero phases suggest a tetravalent state for cobalt, the two phases apparently are prone to accommodate considerable amounts of oxygen vacancies/excess protons (cf. the related $Na_xCoO_{2-\delta}\cdot yH_3O^+\cdot zH_2O$ system [22,23]), which would then induce significant changes in their redox chemistries and structural and physical properties [24,25]. This is presumably because octahedrally coordinated cobalt has a profound reluctancy to get oxidized towards the tetravalent state [26,27]. Actually, for the Ca-based zero ML phase careful chemical and structural characterizations suggested that the phase was best described as $[Ca_{0.85}OH]_{1.16}CoO_2$ or $[Ca_{2-x}(OH)_2]_q[CoO_2]$, and depending on the resultant valence state of cobalt the crystal structure was either monoclinic or orthorhombic [20,21]. For the Sr-counterpart, on the other hand, it was shown that the misfit parameter q depends on the oxygen partial pressure employed for the synthesis [18,28]. Then arises a question how much the two zero phases, $[Sr_2O_2]_q[CoO_2]$ and $[Ca_2O_2]_q[CoO_2]$, have in common. In order to address the question, we have investigated the effects of isovalent Ca-for-Sr substitution in the $[(Sr_{1-x}Ca_x)_2(O,OH)_2]_q[CoO_2]$ system. For the sample synthesis, the closed-ampoule synthesis technique devised for the original synthesis of the first $[Sr_2O_2]_q[CoO_2]$ samples [18] is employed with some modification, i.e. introduction of water vapor pressure. The work hence indirectly underlines the role of protons in stabilizing the $m=0$ ML structure. We moreover show that substitution of the larger Sr by the smaller Ca increases the value of the misfit parameter q from the commensurate value of 0.50 for $x=0$ to 0.52 for $x=0.2$. Effects of the Ca-for-Sr substitution on transport properties are also discussed.

2. Experimental

Samples of $0.0\le x\le 0.2$ of the $[(Sr_{1-x}Ca_x)_2(O,OH)_2]_q[CoO_2]$ system were synthesized employing our sample-encapsulation method [18] using CaO, SrO_2 and Co_3O_4 powders as starting materials. (Here it should be noted that synthesis efforts with $x>0.2$ yielded samples with considerable amounts of impurities.) The SrO_2 powder (freshly home-made *prior* to the use [29,30]) acts in the synthesis as an "internal" oxygen source. The precursor powders were mixed in stoichiometric proportions and pressed into rectangular pellets of $1\times1\times3$ mm^3 which were then placed in a crucible and loaded into an evacuated quartz ampoule together with $SrCl_2\cdot6H_2O$ powder placed in a separate crucible. The function of $SrCl_2\cdot6H_2O$ is to provide with H_2O vapor inside the concealed ampoule. Our observations clearly indicated that the introduction of H_2O into the concealed system promoted the formation of the target zero phase, reducing the amounts of SrO, $SrCO_3$ and Co_3O_4 impurities, typical for the ampoule synthesis route without intentional addition of H_2O [18]. The partial pressure of O_2 inside the ampoule was controlled through adjusting ampoule free space volume and temperature. Various different synthesis temperatures, free-ampoule-volumes and amounts of $SrCl_2\cdot6H_2O$ were tested to reveal that the best results were obtained with the following synthesis parameters: 850 °C, 24 h (slow heating and cooling), ~30 atm of O_2, 30 mol% (as compared to the target zero phase) of $SrCl_2\cdot6H_2O$.

X-ray powder diffraction (XRD) patterns were recorded using Cu$K\alpha$ radiation (Rigaku, RINT-2500 V; equipped with a rotating anode X-ray source). The lattice parameters, a, b_{RS}, c and β, were determined from the XRD data using the Rietveld refinement software JANA2000 [31]. The same structural model with monoclinic $P2_1/m$ space group used earlier for the $x=0.0$ phase [19] was employed for all the samples. The b_H lattice parameter was determined using the [001] incident-beam ED pattern taken with a transmission electron microscope (TEM; Hitachi H-9000NR operating at an accelerating voltage of 300 kV). The misfit parameter, $q=b_H/b_{RS}$, was then determined by using the ED-determined b_H and the XRD-determined b_{RS}. It is worth noting that the value of b_H remains rather constant among the $m=0$ misfit family [19,20,28]. The effects of Ca-for-Sr substitution on the morphology of the sintered product pellet surface were observed with scanning electron microscopy (SEM; Hitachi S-6500).

Electrical resistivity in the temperature range from 4 to 300 K was measured for the samples using a four-probe technique (Quantum Design, PPMS). The thermoelectric power was measured in the temperature range of 5–280 K with a steady-state technique. Magnetization was recorded from 2 to 300 K with a SQUID magnetometer (Quantum Design, MPMS-XL) both in the zero-field-cooled (ZFC) and field-cooled (FC) modes under 10 kOe.

3. Results and discussion

Our ampoule synthesis yielded nearly single-phase $[(Sr_{1-x}Ca_x)_2(O,OH)_2]_q[CoO_2]$ samples up to $x=0.2$ although peaks due to trace

amounts of $SrCO_3$ and Co_3O_4 impurity phases were seen for all the samples; X-ray diffraction patterns of the samples are shown in Fig. 2. Most of the XRD peaks were readily indexed within the monoclinic $P2_1/m$ unit-cell employed for the parent $[Sr_2O_2]_q[CoO_2]$ phase in our original works [18,19]. Table 1 summarizes the lattice parameters of the present $x=0.0$, 0.05, 0.10 and 0.20 samples determined from the XRD patterns. Fig. 3 displays SEM images for some of the samples. It is seen that the degree of sintering is somewhat enhanced for the Ca-substituted samples. The grain size is of the order of 5–10 μm.

Careful observation of the XRD data given in Fig. 2 reveals that the non-(00l) reflections become more significantly rounded with increasing Ca-for-Sr substitution level, x. This is apparently a consequence of peak splitting, more clearly visible for the high-angle reflections. The splitting presumably has its origin in the translational modulations of the atomic positions due to the emerging inter-layer mismatch. The modulations tend to be more pronounced in the rock-salt block as compared to the more rigid and tightly packed $[CoO_2]$ layer [32]. Fig. 4(a) shows the contraction of the lattice parameters, a, b_{RS} and c, with increasing x (hollow symbols), as determined through XRD. For comparison we have also included the lattice parameters reported for the monoclinic $x=1.0$ end phase (filled symbols) by Shizuya et al. [21]. With increasing x, the lattice contracts more strongly along the b_{RS} axis than along the a and c axes. Fig. 4(b) moreover illustrates that while the $x=0.0$ pristine phase has a commensurate match between its b_H and b_{RS} lattice parameters ($q=b_H/b_{RS}=0.50$), substitution of Sr by the smaller Ca contracts the rock-salt layer more efficiently, thus increasing the q value and creating some finite degree of misfitness between the $[(Sr_{1-x}Ca_x)_2(O,OH)_2]$ and $[CoO_2]$ blocks. The same is illustrated with ED patterns (see the insets of Fig. 4(b)), where the deviation of the q value from 0.5 is seen as shifts of the reflection spots due to the RS block along the b-axis direction from those present in the $x=0.0$ sample.

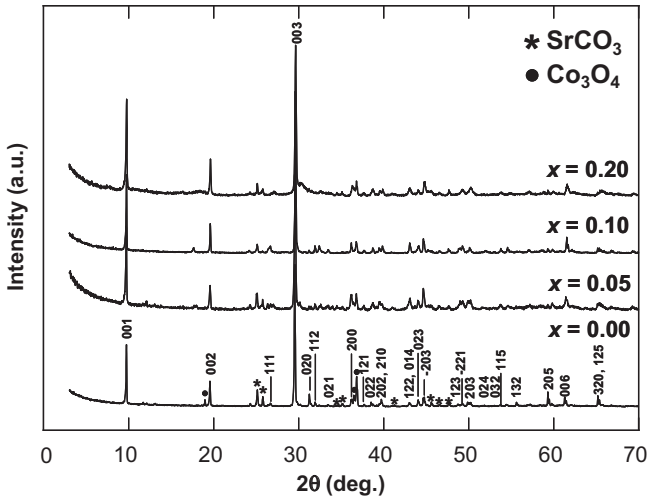

Fig. 2. XRD patterns for the $[(Sr_{1-x}Ca_x)_2(O,OH)_2]_q[CoO_2]$ samples.

Table 1
Lattice parameters, a, b_{RS}, c and β (from XRD data), and the misfit parameter q (from ED data) for the $[(Sr_{1-x}Ca_x)_2(O,OH)_2]_q[CoO_2]$ samples.

Sample	a (Å)	b_{RS} (Å)	c (Å)	β (deg)	q
$x=0.00$	4.983	5.593	9.091	96.27	0.50
$x=0.05$	4.981	5.540	9.083	96.27	0.51
$x=0.10$	4.978	5.506	9.080	96.26	0.51
$x=0.20$	4.964	5.422	9.077	96.25	0.52

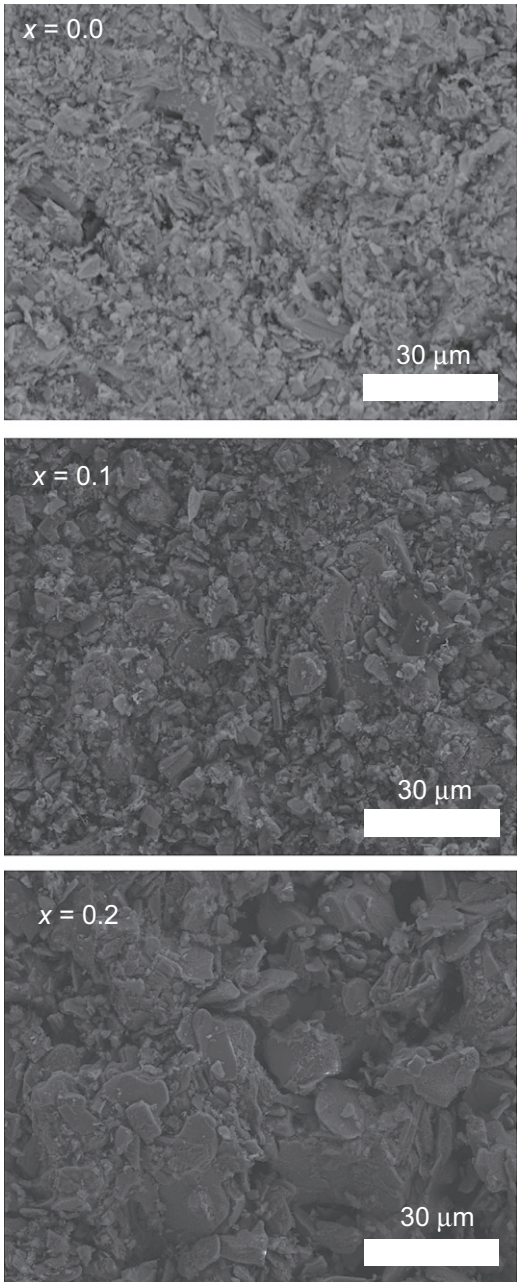

Fig. 3. SEM images for the $x=0.0$, 0.1 and 0.2 samples of $[(Sr_{1-x}Ca_x)_2(O,OH)_2]_q[CoO_2]$.

From Figs. 4(a) and (b), the a and b_{RS} parameters and the q value of our samples show almost linear coincidence with the monoclinic $x=1.0$ sample by Shizuya et al. [21]. For parameter c, monotonic but slightly off-linear decrease between $x=0.2$ and 1.0 is seen. From previous studies it is known that hydrogen ions are necessary for synthesizing the $[Ca_2(O,OH)_2]_q[CoO_2]$ phase. Our present study points out that this is most likely the case even with the present "$[Sr_2O_{2-\delta}]_q[CoO_2]$-type [18] phases", though the affinity for hydrogen inclusion seems to be less pronounced than in the case of the Ca-analog. The essentially linear lattice contraction revealed here upon the Ca-for-Sr substitution provides us with strong indication towards the fact that the "$[Sr_2O_{2-\delta}]_q[CoO_2]$" and "$[Ca_2(OH)_2]_q[CoO_2]$" zero phases are members of the same $[(Sr_{1-x}Ca_x)_2(O,OH)_2]_q[CoO_2]$ system.

For all of our $[(Sr_{1-x}Ca_x)_2(O,OH)_2]_q[CoO_2]$ samples electrical resistivity shows metallic behavior at high temperatures and then

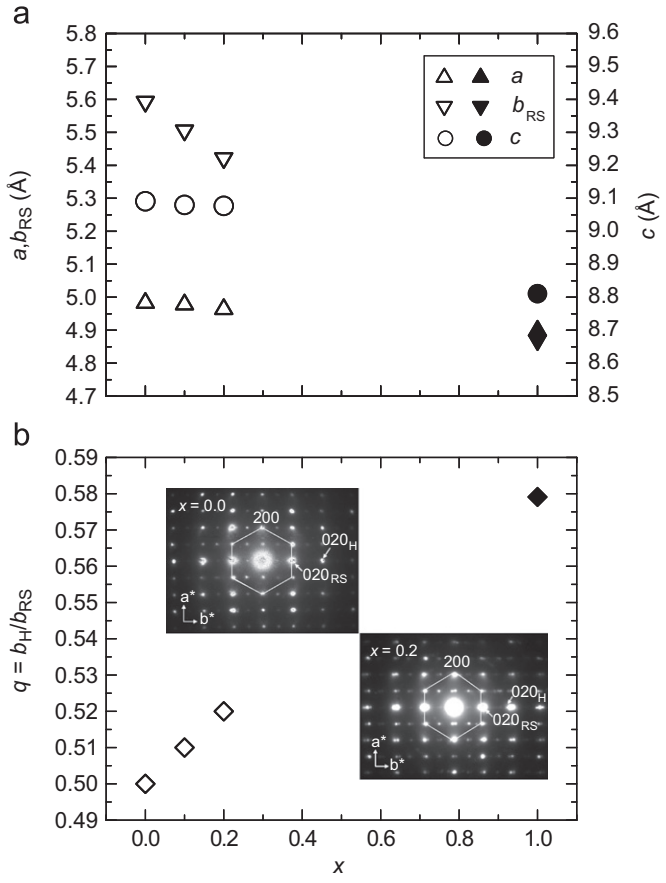

Fig. 4. (a) Evolution of the lattice parameters and (b) the misfit parameter q with the substitution degree (insets: ED images along the [001] incident beam direction to demonstrate the emerging misfit along the b-axis direction). Hollow symbols represent data for the $[(Sr_{1-x}Ca_x)_2(O,OH)_2]_q[CoO_2]$ samples of this study; filled symbols represent data for the sample with $[Ca_{1.7}O_{2.1}H_{2.4}]_{0.58}[CoO_2]$ stoichiometry reported by Shizuya et al. [21].

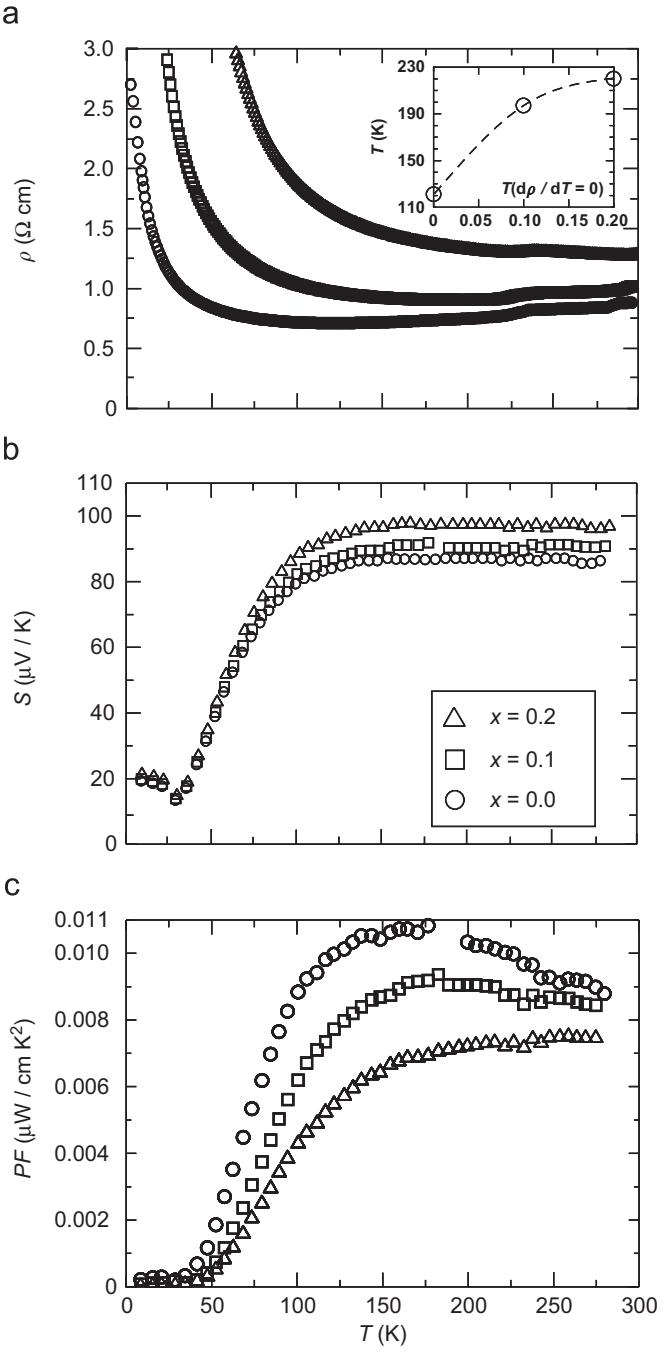

Fig. 5. Temperature dependence of (a) resistivity (inset: insulator to metal turning point), (b) Seebeck coefficient, and (c) power factor for the x=0.0, 0.1 and 0.2 samples of $[(Sr_{1-x}Ca_x)_2(O,OH)_2]_q[CoO_2]$.

exhibits an upturn as temperature decreases (see Fig. 5(a)). Here it should be noted that a similar upturn is seen for most of the known ML cobalt oxides [35,42–44]. Both the absolute resistivity and the upturn temperature (see the inset in Fig. 5(a)) increase with increasing x. SEM images displayed in Fig. 3 confirm this observation to be intrinsic to the $[(Sr_{1-x}Ca_x)_2(O,OH)_2]_q[CoO_2]$ system and not related to the grain boundary effects, as the sintering seems to be rather enhanced for the Ca-substituted samples. The Seebeck coefficient displayed in Fig. 5(b) remains positive over the temperature range studied, indicating holes as the major charge carriers. The S value shows a levelling-off behavior above ~175 K, which is rather independent of x. However, the levelled-off maximum S value increases with increasing x (from 87 μV/K for $x=0.0$ to 97 μV/K for $x=0.2$).

Shizuya et al. [24] have observed similar transport behavior for their $[Ca_2(O,OH)_2]_q[CoO_2]$ samples. In their work there is no clear upturn temperature, but decreasing cobalt valence is coupled with a more sluggish increase in resistivity with higher overall value and a higher levelled-off maximum Seebeck coefficient (from 100 μV/K with Co(+3.16) to 110 μV/K with Co(+3.08)). Thus, it is suspected that in the $[(Sr_{1-x}Ca_x)_2(O,OH)_2]_q[CoO_2]$ system, as x increases, the ratio of OH^- to O^{2-} at the (O,OH) site increases to decrease the average cobalt valence (and to increase the ρ and S values).

Ishiwata et al. [28] have discussed the dependency of the room-temperature Seebeck coefficient on the misfit parameter q among known ML cobalt oxides. In Fig. 6 we redraw their original figure completed with our present data which lie elegantly right on the straight correlation line given in [28]. Here we like to emphasize that the Seebeck coefficient also strongly depends on the carrier concentration/Co valence which may not be exactly the same for all the samples in Fig. 6. However, from Fig. 6 we may conclude that within the framework of the misfit layered cobalt oxides $[M_mA_2O_{m+2}]_q[CoO_2]$, the misfit parameter q is one of the prime factors in adjusting the Seebeck coefficient. From the thermoelectric application point of view, the increase in the Seebeck coefficient seen in our $[(Sr_{1-x}Ca_x)_2(O,OH)_2]_qCoO_2$ system with increasing x is however relatively weak as compared to that in resistivity such that the thermoelectric power factor ($PF=S^2/\rho$) rather declines as the isovalent Ca-for-Sr substitution proceeds (see Fig. 5(c)).

Finally, in Fig. 7 we show magnetic susceptibility data for our $[(Sr_{1-x}Ca_x)_2(O,OH)_2]_q[CoO_2]$ samples. For the parent $x=0.0$ sample

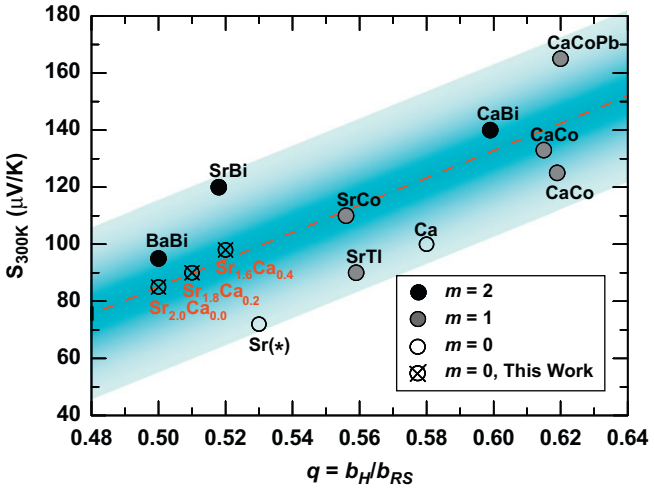

Fig. 6. Seebeck coefficient at 300 K vs. misfit ratio among selected misfit-layered cobalt oxides with a monoclinic lattice [28]. Our samples are highlighted in red. CaCoPb: $[Ca_2Co_{0.6}Pb_{0.4}O_3]_{0.62}CoO_2$ [34], CaCo: $[Ca_2CoO_3]_{0.62}CoO_2$ [35,36] CaBi: $[Ca_2Bi_{1.7}Co_{0.3}O_4]_{0.57}CoO_2$ [37] SrCo: $[Sr_2CoO_3]_{0.56}CoO_2$ (5% Ti-doped) [38], SrTl: $[Sr_{1.8}Tl_{0.71}O_{3-\delta}]_{0.56}CoO_2$ [39], Sr(*): $[Sr_2O_{2-\delta}]_{0.53}CoO_2$ [28], SrBi: $[Sr_2Bi_2O_4]_{0.52}CoO_2$ [40], BaBi: $[Ba_{1.8}Co_{0.2}Bi_2O_4]_{0.5}CoO_2$ [41]. (For interpretation of the references to color in this figure legend, the reader is referred to the web version of this article.)

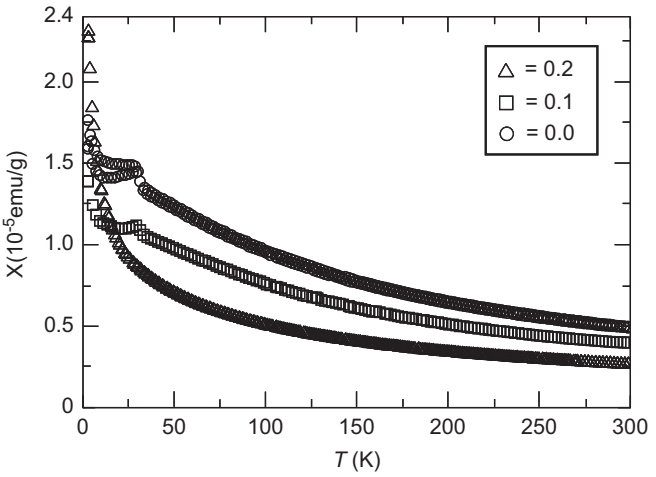

Fig. 7. Magnetic susceptibility with respect to temperature for the $x=0.0$, 0.1 and 0.2 samples of $[(Sr_{1-x}Ca_x)_2(O,OH)_2]_q[CoO_2]$.

an anomaly is seen around 35 K, which we attributed in our original work to trace amounts of antiferromagnetic Co_3O_4 impurity ($T_N \approx 33$ K [33]). With increasing Ca-for-Sr substitution level, the anomaly gets weaker. Also seen from Fig. 7 (and from the $1/\chi$ versus T plots not shown here) is that the high-temperature behavior of magnetization gradually approaches the Curie–Weiss behavior. Note that the $x=1.0$ end member, $[Ca_2(O,OH)_2]_q[CoO_2]$, was reported to obey a Curie–Weiss behavior [24]. Tentatively we tend to believe that, once the lattice coherency strain (in the $x=0.0$ phase) is released upon Ca substitution the somewhat strain-constrained spin arrangement may have been relaxed. It is clear that more precise magnetic-property analyses are required for a more complete understanding.

4. Conclusion

In this work isovalent Ca-for-Sr substitution in the $[(Sr_{1-x}Ca_x)_2(O,OH)_2]_q[CoO_2]$ system was successfully made for the first time. For stabilizing the phases of the system both H_2O vapor and elevated oxygen partial pressure were found to be essential. This points out that boosting the cobalt valence is necessary for synthesizing the phases, though the affinity for hydrogen inclusion seems to be less pronounced than in the case of the $[Ca_2(O,OH)_2]_q[CoO_2]$ phase formerly reported.

While the $[Sr_2O_2]_q[CoO_2]$ phase (with $x=0.0$) has a coincidentially commensurate match ($q=0.5$) between the $[CoO_2]$ layer and the rock-salt type block, Ca substitution for Sr induces misfit between them. Such substitution increases the Seebeck coefficient. However, the simultaneous increase in resistivity outweighs this benefit, as is observable from the decrease in the thermoelectric power factor. The overall transport characteristics of the system drift from metallic towards semi-conductive. At the same time spins constrained with coherency strain tend to be relaxed when the lattice becomes incommensurate as the Ca-for-Sr substitution proceeds. An earlier conclusion pointing out the linear dependency between the Seebeck coefficient and the misfit parameter is supported by the present results.

Acknowledgments

The present work was supported by Tekes (no. 1726/31/07), Academy of Finland (nos. 126528 and 130352) and the Finnish Foundation for Technology Promotion.

References

[1] P. Boullay, B. Domengès, M. Hervieu, D. Groult, B. Raveau, Chem. Mater. 8 (1996) 1482.
[2] P. Boullay, R. Seshadri, F. Studer, M. Hervieu, D. Groult, B. Raveau, Chem. Mater. 10 (1998) 92.
[3] I. Terasaki, Y. Sasago, K. Uchinokura, Phys. Rev. B 56 (1997) R12685.
[4] M. Shikano, R. Funahashi, Appl. Phys. Lett. 82 (2003) 1851.
[5] N.V. Nong, C.J. Liu, M. Ohtaki, J. Alloys Compd. 491 (2010) 53.
[6] Y. Liu, Y. Lin, L. Jiang, C.W. Nan, Z. Shen, J. Electroceram. 21 (2008) 748.
[7] J.J. Shen, X.X. Liu, T.J. Zhu, X.B. Zhao, J. Mater. Sci. 44 (2009) 1889.
[8] T. Motohashi, Y. Katsumata, T. Ono, R. Kanno, M. Karppinen, H. Yamauchi, Chem. Mater. 19 (2007) 5063.
[9] S. Kawasaki, T. Motohashi, K. Shimada, T. Ono, R. Kanno, M. Karppinen, H. Yamauchi, G.Q. Zheng, Phys. Rev. B 79 (2009) 220514.
[10] T. Motohashi, T. Ono, Y. Sugimoto, Y. Masubuchi, S. Kikkawa, R. Kanno, M. Karppinen, H. Yamauchi, Phys. Rev. B 80 (2009) 165114.
[11] F.C. Chou, E.T. Abel, J.H. Cho, Y.S. Lee, J. Phys. Chem. Solids 66 (2005) 155.
[12] S. Venkatraman, A. Manthiram, Chem. Mater. 14 (2002) 3907.
[13] W. Koshibae, K. Tsutsui, S. Maekawa, Phys. Rev. B 62 (2000) 6869.
[14] Y. Miyazaki, Solid State Ionics 172 (2004) 463.
[15] M. Karppinen, H. Fjellvåg, T. Konno, Y. Morita, T. Motohashi, H. Yamauchi, Chem. Mater. 16 (2004) 2790.
[16] Y. Morita, J. Poulsen, K. Sakai, T. Motohashi, T. Fujii, I. Terasaki, H. Yamauchi, M. Karppinen, J. Solid State Chem. 177 (2004) 3149.
[17] Y. Tanaka, T. Fujii, M. Nakanishi, Y. Kusano, H. Hashimoto, Y. Ikeda, J. Takada, Solid State Commun. 141 (2007) 122.
[18] H. Yamauchi, K. Sakai, T. Nagai, Y. Matsui, M. Karppinen, Chem. Mater. 18 (2006) 155.
[19] T. Nagai, K. Sakai, M. Karppinen, T. Asaka, K. Kimoto, A. Yamazaki, H. Yamauchi, Y. Matsui, J. Solid State Chem. 179 (2006) 1898.
[20] M. Shizuya, M. Isobe, Y. Baba, T. Nagai, M. Osada, K. Kosuda, S. Takenouchi, Y. Matsui, E. Takayama-Muromachi, J. Solid State Chem. 180 (2007) 249.
[21] M. Shizuya, M. Isobe, Y. Baba, T. Nagai, Y. Matsui, E. Takayama-Muromachi, J. Solid State Chem. 179 (2006) 3974.
[22] K. Takada, H. Sakurai, E. Takayama-Muromachi, F. Izumi, R.A. Dilanian, T. Sasaki, Nature 422 (2003) 53.
[23] M. Karppinen, I. Asako, T. Motohashi, H. Yamauchi, Chem. Mater. 16 (2004) 1693.
[24] M. Shizuya, M. Isobe, E. Takayama-Muromachi, J. Appl. Phys. 102 (2007) 023704.
[25] Y. Ikedo, J. Sugiyama, H. Nozaki, P.L. Russo, D. Andreica, A. Amato, M. Månsson, M. Shizuya, M. Isobe, E. Takayama-Muromachi, Physica B 404 (2009) 607.
[26] M. Karppinen, I. Asako, T. Motohashi, H. Yamauchi, Phys. Rev. B 71 (2005) 092105.
[27] L. Karvonen, H. Yamauchi, M. Karppinen, Chem. Mater. 20 (2008) 7143.
[28] S. Ishiwata, I. Terasaki, Y. Kusano, M. Takano, J. Phys. Soc. Jpn. 75 (2006) 104716.
[29] T. Kawashima, E. Takayama-Muromachi, Physica C 267 (1996) 106.
[30] M. Ushiki, T. Motohashi, H. Yamauchi, M. Karppinen, Physica C 378–381 (2002) 167.

[31] V. Petricek, M. Dusek, The Crystallographic Computing System JANA2000, Institute of Physics, Praha, Czech Republic,, 2000.
[32] M. Isobe, M. Onoda, M. Shizuya, M. Tanaka, E. Takayama-Muromachi, J. Am. Chem. Soc. 129 (2007) 14585.
[33] W. Kündig, M. Kobelt, H. Appel, G. Constabaris, R.H. Lindquist, J. Phys. Chem. Solids 30 (1969) 819.
[34] A. Maignan, S. Hébert, D. Pelloquin, C. Michel, J. Hejtmanek, J. Appl. Phys. 92 (2002) 1964.
[35] Y. Miyazaki, K. Kudo, M. Akoshima, Y. Ono, Y. Koike, T. Kajitani, Jpn. J. Appl. Phys. 39 (2000) L531.
[36] A.C. Masset, C. Michel, A. Maignan, M. Hervieu, O. Toulemonde, F. Studer, B. Raveau, Phys. Rev. B 62 (2000) 166.
[37] A. Maignan, S. Hébert, M. Hervieu, C. Michel, D. Pelloquin, D. Khomskii, J. Phys.: Condens. Matter 15 (2003) 2711.
[38] D. Pelloquin, S. Hebért, A. Maignan, B. Raveau, Solid State Sci. 6 (2004) 167.
[39] S. Hébert, S. Lambert, D. Pelloquin, A. Maignan, Phys. Rev. B 64 (2001) 172101.
[40] T. Fujii, I. Terasaki, T. Watanabe, A. Matsuda, Jpn. J. Appl. Phys. 41 (2002) L783.
[41] M. Hervieu, A. Maignan, C. Michel, V. Hardy, N. Créon, B. Raveau, Phys. Rev. B 67 (2003) 045112.
[42] W. Kobayashi, H. Muguerra, S. Hébert, D. Grebille, A. Maignan, J. Phys.: Condens. Matter 21 (2009) 235404.
[43] T. Yamamoto, K. Uchinokura, I. Tsukada, Phys. Rev. B 65 (2002) 184434.
[44] Y. Miyazaki, T. Miura, Y. Ono, T. Kajitani, Jpn. J. Appl. Phys. 41 (2002) L849.